High Sensing Accuracy Realisation with Millimetre/sub-Millimetre Resolution in Optical Frequency Domain Reflectometer

Zhen Guo, Jize Yan, Gaoce Han, David Greenwood, James Marco and Yifei Yu

***Abstract*— By effectively suppressing the nonlinear sweep noise and random range of wavelength sweep in the optical frequency domain reflectometer, the theoretical spatial resolution and uniform sweep distribution are delivered for high sensing accuracy. A strain accuracy of ±0.51 με is realised with a 5 mm sensing resolution, while the accuracy is ±5.89 με with a 1 mm sensing resolution. Theoretical limitation between the strain accuracy and sensing resolution is further studied for the sub-millimetre resolution sensing. It is found that signal to noise ratio and frequency bandwidth of the calculated cross-correlation are critical factors in measuring accuracy. Increasing the sweep range can provide a better spatial frequency step for a high signal to noise ratio in the cross-correlation. With a 130 nm sweep range, the measurement accuracy is limited to ±19.31 με with a 0.5 mm sensing resolution. Besides, for the long-distance sensing of 104m, the measurement accuracy is ±8.72 με with a 1 mm sensing resolution.**

***Index Terms*— Optical frequency domain reflectometer, nonlinear wavelength sweep, accuracy, sensing resolution**

I. Introduction

Optical frequency domain reflectometer (OFDR) is one of intrinsic-scattering based distributed optical fibre sensing (Rayleigh, Brillouin, et al.)[1-3]. Due to the excellent spatial resolution and dynamic range by tuning the laser wavelength, OFDR is becoming one of the most attractive ways to realise high precision sensing. It is mainly used in the optical components metrology for the measurement of transmission loss and link diagnosis in the optical network [4]. Recently, some battery management systems (BMS) employed this distributed sensing to measure the temperature difference across the cell and the hot region movement in real-time [5-7]. Besides the battery's surface temperature/strain sensing, optical fibre has the potential advantage of being implanted inside the battery to estimate the state of health/power/charge more accurately. Moreover, the increasing number of battery cells to hundreds or even thousands in one battery pack makes the OFDR with high spatial resolution the preferable candidate in the distributed optical fibre sensing in the battery monitor system.

With further demand for sensing resolution, such as μm-level optical components metrology and mm-level strain/temperature monitoring, the trade-off between measurement accuracy and sensing resolution in the OFDR needs to be considered [8]. As the "uncertainty principle", the accuracy and sensing resolution cannot be improved simultaneously beyond the theoretical limit [9-11]. Based on the finite bandwidth measurement of the complex reflection and cross-correlation calculation between the reference and measurement spectrums, theoretical accuracy and sensing resolution must be guaranteed by the precise position information and exact the same physical fibre segment between two times measurements.

The nonlinear wavelength sweep in the coherent OFDR will expand the spatial resolution and blur the position information. An auxiliary interferometer is usually used to estimate and compensate for the nonlinear sweep noise [12]. A diverse polarisation method is proposed to obtain a 22 μm spatial resolution over 35 meters of optical length [13]. Hilbert transform-based correction paves another way to suppress the nonlinear sweep by getting the instantaneous sweep distribution [14]. In the previous study, an equal frequency resample is proposed for the theoretical spatial resolution. With a 130nm sweep range, a 12.1 μm spatial resolution is obtained with 1.9-meter optical fibre, while the spatial resolution is 21.3 μm with 191-meter optical fibre [15]. Besides the nonlinear sweep noise, a position-deviation compensation is proposed to maintain the cross-correlation of the Rayleigh spectrum for a 0.5 mm resolution [16]. Local similar characteristics of the Rayleigh spectrum are introduced and discussed to realise a 3 mm long fibre gauge [17]. The measurement strain accuracy is enhanced to 3 με with the spatial resolution of 1 cm by the spectrum interpolation technique [18]. Recently, an image de-noising technique has been applied to improve optical distributed sensing, especially the ultimate sensing resolution. Five to tenfold suppression of measurement deviation is delivered with a 3 mm gauge length [19]. Using the distance compensation and image wavelet de-noising, a 2.56 mm resolution and four times accuracy enhancement are achieved

Manuscript received XXXX, 2021; revised XXXX, 2021; accepted XXXX, 2021. Date of publication XXXX, 2021; date of current version XXXX, 2021.

This work was supported by the High Value Manufacturing Catapult and the Engineer and Physical Sciences Research Council. (*Corresponding author: Yifei Yu.)*

Z. Guo, G. Han, D. Greenwood, J. Marco, Y. Yu are with Warwick Manufacturing Group (WMG), University of Warwick, Coventry, CV4 7AL, United Kingdom; (e-mail: Zhen.Guo@warwick.ac.uk; Gaoce.Han@warwick.ac.uk; D.Greenwood@warwick.ac.uk; James.Marco@warwick.ac.uk; Yifei.Yu.1@warwick.ac.uk)

J.Yan, G. Han are with Electronics and Computer Science (ECS), University of Southampton, Southampton, SO17 1BJ, United Kingdom; (e-mail: J.Yan@southampton.ac.uk)

[20]. But the image de-noise also brings out the extra data process and hardware consumption.

The experimental relationship between accuracy and sensing resolution in OFDR hasn't been discussed thoroughly. As we have obtained the theoretical-level spatial resolution in the previous work [15], we further investigate the sensing accuracy with the ultimate sensing resolution. In this paper, the influence of nonlinear sweep noise and random wavelength sweep range of the laser are studied in the next section. Then, by equal frequency resample and sweep range correction, a 5 mm resolution with ±0.51 με accuracy is experimentally realised. The theoretical relationship between accuracy and spatial resolution is also discussed with various sweep ranges. In the last part, an ultimate 0.5 mm resolution and a long-distance distributed sensing of 100 m are represented to demonstrate the efficient suppression of the nonlinear sweep noise and randomly distributed sweep range for the high accuracy with the sub-millimetre resolution.

II. PRINCIPLE

A. OFDR distributed sensing

Coherent OFDR is composited of a tunable laser source (TLS) and an interferometer (Fig. 1(a)). There is a local oscillator (LO) in the reference arm and fibre under test (FUT) in the sensing arm. The beating signal of reference and sensing arms is detected by a photodetector (PD). With a wavelength sweep speed γ of the laser source, the interference between the position z along the FUT and LO can be expressed as:

$$I(t)=E_0^2\left\{1+\frac{2R_{LO}R_{RBS}}{R_{LO}+R_{RBS}}\cos\left[2\pi\left(\nu_0\tau_z+\gamma\tau_z t-\frac{1}{2}\gamma\tau_z^2+\phi_n(t,\tau_z)\right)\right]\right\} \quad (1)$$

where R_{LO} and R_{RBS} are the intensity coefficients of the LO and the Rayleigh backscattering light, respectively; $\phi_n(t)$ is the phase noise; τ_z is the optical time delay between the position z and the reference arm. Thus, a position of z along the FUT would correspond to the beat frequency $\gamma\tau_z$. Due to the limited frequency sweep range, the theoretical spatial resolution limitation of OFDR is $\Delta z = c/2n\upsilon_{scan}$, where c is the light speed, n is the index of fibre and υ_{scan} is the laser sweep range.

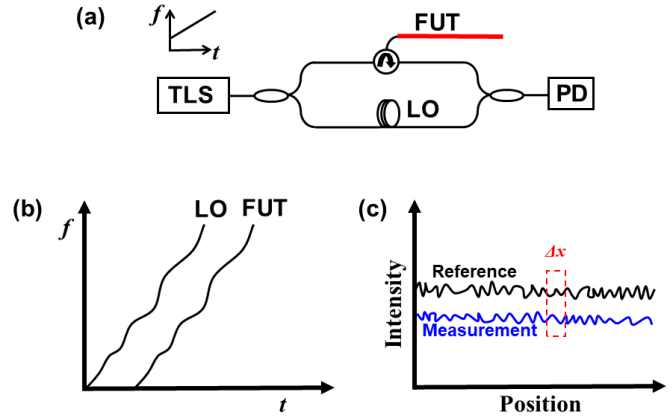

Fig.1 (a) Schematic diagram of OFDR (b) Nonlinear wavelength sweep (c) Spatial frequency filtering of Δx in the reference and measurement sensing

The linear wavelength sweep provides the position information along with the fibre under test. To realise temperature/strain sensing, the variation of the randomly distributed permittivity in the fibre is introduced by filtering the specific spatial frequency components [8]:

$$\int_{-\Delta\beta}^{\Delta\beta} I_d(\beta-\beta_0)\exp(-i\beta x)d\beta = E_0^2 r\frac{c\pi\beta_0}{ni}\Delta\bar{\varepsilon}^*\left(z_0+\frac{x}{2}\right) \quad (2)$$

where β_0 is the detected wave number, $\Delta\beta$ is the range of measurement wave number, r is the reflectivity of the Rayleigh scattering, $\Delta\varepsilon$ is the variation of permittivity at the certain spatial frequency components. This process is usually regarded as the slidewindow filtering in the OFDR demodulation (Fig. 1(c)). Then, a cross-correlation of the spectrums between the strained section and the same section without strain is carried out to compute the frequency shift of the applied strain.

B. Nonlinear sweep noise

Due to the nonlinear sweep noise (Fig. 1(b)), beating frequency between the LO and FUT will have random frequency deviation to deteriorate the spatial resolution. An auxiliary interferometer is usually employed to suppress the nonlinear sweep. Zero-crossing points in interference fringes in the auxiliary interferometer are usually used to resample the OFDR signals to compensate for the sweep nonlinearity. But the estimation accuracy is limited by the optical fibre length. By introducing high order Taylor components of frequency distribution to compensate for this nonlinear sweep noise, we proposed an equal frequency resample to efficiently suppress the nonlinear sweep noise for better spatial resolution [15]. The experimental result is shown in Fig. 2(a). The corresponding length of FUT is about 6 m. The peaks around 1 m and 3 m are optical fibre connectors. With a sweep range of 130 nm, the theoretical spatial resolution is 6.2 μm. The measured spatial resolution with zero-crossing resample is about 0.01m, while the measured spatial resolution of the interpolation fitting with the proposed method is about 15.6 μm (Fig. 2(b)). The realisation of such a theoretical-level resolution illustrates the effective suppression of nonlinear noise and helps to improve the signal to noise ratio of the spectrum signal.

C. Random distribution of the wavelength sweep range

Besides the nonlinear sweep noise, the following processes of OFDR demodulation, as filtering of specific spatial frequency components and cross-correlation, have to be guaranteed by precisely the same physical optical fibre segment between the two times comparison (reference and measurement). The corresponding position information is determined by the overall sweep range and the corresponding frequency interval. The frequency interval is compensated by the the equal frequency resample. Therefore, the distribution of the sweep range is investigated for further performance. An interferometer and a Hilbert transform can measure the distribution of one wavelength sweep. The Hilbert transform can obtain the instantaneous optical frequency distribution [14]:

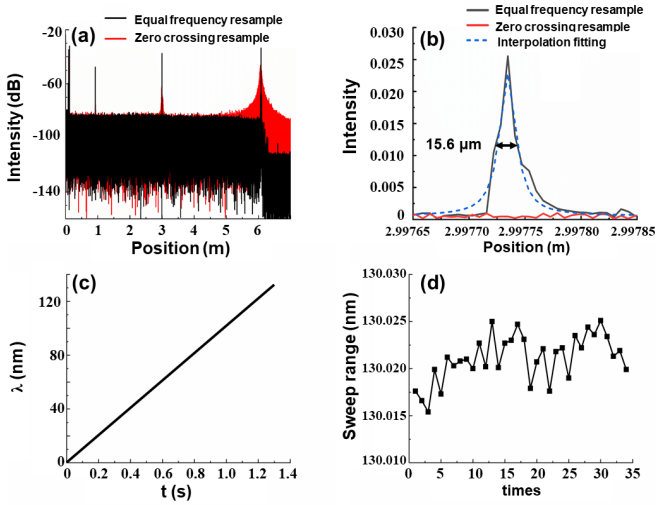

Fig.2 (a) Spectrum distribution of a 6 meter fibre under test (b) Spatial resolution under the sweep range of 130 nm (c) The distribution of wavelength sweep at 100 nm/s sweep speed (d) Random deviation of sweep range with a claimed 130 nm range

$$v(t)=\arctan\left(\frac{H\{I(t)\}}{I(t)}\right)\Big/(2\pi\tau) \tag{3}$$

where $H\{\ \}$ is the Hilbert transform and $I(t)$ is the signal from the interferometer. The experimental distribution of a laser wavelength sweep is shown in Fig. 2(c). The claimed sweep range is 130 nm, while the measured sweep range is 130.0176 nm. The random distribution of the sweep range is shown in Fig. 2(d). The mean value of measured sweep ranges is about 130.021 nm, while the deviation is limited to 0.01 nm. The discrete Fourier transform of the OFDR interference signal is the function of space with a step size of theoretical spatial resolution. Though such deviation has little effect on the theoretical spatial resolution, with an increasing fibre length, this deviation can be accumulated. The sweep range deviation of 0.01 nm would induce about 12 points offset at 1 m fibre length.

Therefore, to compare the exact spectrum of the same fibre segment between the reference and measurement, the random deviation of the sweep range has to be compensated. The Fourier transforms of the two times measurements are:

$$\begin{aligned}\tilde{I}_{ref}&=\frac{1}{N_{ref}}\sum_{j=0}^{N_{ref}-1}I_{ref}\exp\left(-imj\frac{2\pi}{N_{ref}}\right)\quad at\ \text{step}\ \Delta z_{ref}=\frac{c}{2\pi\upsilon_{ref}}\\ \tilde{I}_{sen}&=\frac{1}{N_{sen}}\sum_{j=0}^{N_{sen}-1}I_{sen}\exp\left(-imj\frac{2\pi}{N_{sen}}\right)\quad at\ \text{step}\ \Delta z_{sen}=\frac{c}{2\pi\upsilon_{sen}}\end{aligned} \tag{4}$$

The derived sweep range υ_{sen} should be modified and calibrated with υ_{ref} for the identical step Δz. Therefore, the theoretical spatial resolution by equal frequency resample provides a precise frequency step. The compensation of the random sweep range provides the absolute value of the spatial frequency components.

III. Experiment and Discussion

An OFDR-based distributed strain sensing is shown in Fig.3 (a). The output power of the tunable laser source (Santec-TSL-550) is 9.5dBm, which is split by a 99:1 coupler. The sweep wavelength speed is 100 nm/s with a range from 1500 nm to 1630 nm. 1% light launches into the auxiliary interferometer for the nonlinear sweep estimation and compensation. The corresponding length of the optical path delay is 190m. The other 99% light launches into the main interferometer, where the fibre under test lies at the second port of the circulator. Another 99:1 coupler is used to guarantee the intensity of Rayleigh backscattering light from the fibre under test. The variable optical attenuator (VOA) and two 99:1 couplers are used to improve interference visibility. The signals of auxiliary and main interferometers are detected by photodetectors and digitised by the DAQ (Picoscope 6404D) at the sample rate of 78.13 MHz.

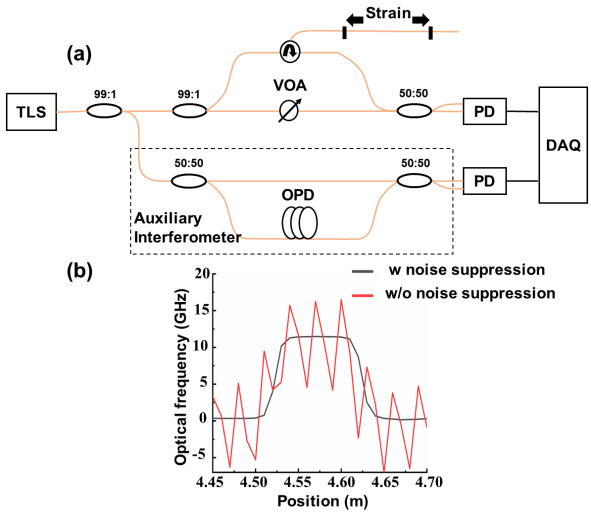

Fig.3 (a) Experimental setup (b) Experimental results of distributed strain sensing with proposed noise suppression and without noise suppression. The applied strain is 100 με and the sensing resolution is 0.01m.

The equal frequency resample could provide a theoretical spatial resolution in the auxiliary interferometer under a 130 nm sweep range. Meanwhile, the sweep ranges of the reference and

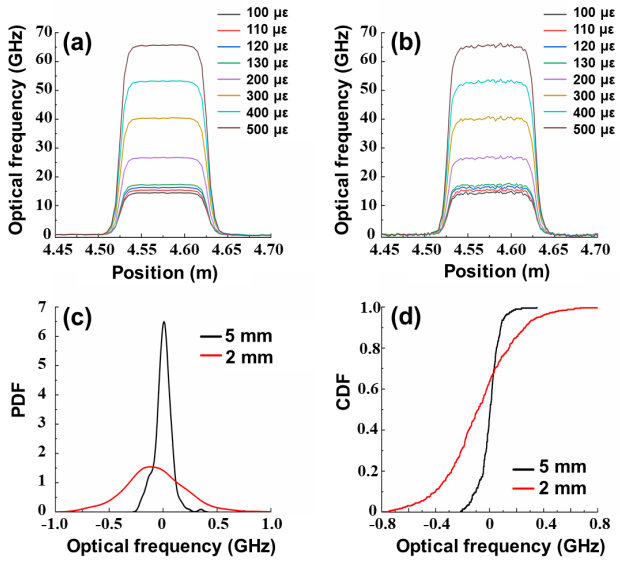

Fig.4 (a) Optical frequency shift distribution with the sensing resolution of 5 mm (b) Optical frequency shift distribution with the sensing resolution of 2 mm (c) Probability density function (PDF) of the random frequency shifts (d) Cumulative distribution function (CDF) of the random frequency shifts

measurement are obtained by the Hilbert transform, which will be calibrated for the same step size in the spatial frequency domain. Then the slidewindow is carried out to filter the same frequency components for the cross-correlation. Fig.3 (b) represents the comparison of distributed sensing with and without noise suppression. The sensing resolution is 0.01 m. The proposed method could efficiently suppress the nonlinear sweep noise and random wavelength range for accurate measurements.

With a 130 nm sweep range and a 100 nm/s sweep speed, the distributed frequency shift with various applied strain is further shown in Fig. 4. The fibre segment between 4.53 m and 4.63 m is fixed on the strain-applied stage. Fig. 4(a) and (b) represent the frequency shift distribution under a 5 mm sensing resolution and 2 mm sensing resolution, respectively. With the increasing applied strain, the frequency shift is changing linearly at the corresponding fibre section. The theoretical step size of the 130 nm sweep range is 6.3 μm. Thus, there are 793 points during one spatial filtering with a 5 mm sensing resolution and 317 points with a 2 mm sensing resolution. The decreasing number of points will deteriorate the signal to noise ratio of the following process of cross-correlation. Therefore, compared to the 5 mm sensing resolution, the measured frequency shift of the 2 mm sensing resolution has apparent random deviations. To quantify such measurement uncertainty, the probability density function (PDF) and the cumulative distribution function (CDF) are employed to represent the sensing accuracy. Mounts of frequency shifts of the strained and un-strained area are measured multiple times for the random deviation investigation. The frequency shift of the strained area needs to subtract the mean value caused by the applied strain. In Fig. 4(c), the PDF bandwidth of the 5 mm resolution is much narrower than that of 2 mm, indicating the more stable strain measurement with a larger resolution. The measurement accuracy is defined as the 2σ standard deviation of the random frequency shift. This accuracy represents the closeness of measurements to a specific value of applied strain. Therefore,

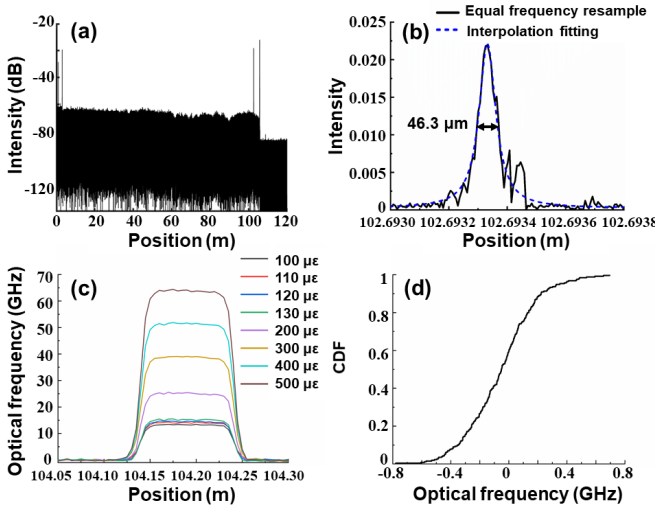

Fig.5 (a) Spectrum distribution of a 104 meter fibre under test (b) a 46.3 μm spatial resolution under the sweep range of 130 nm (c) Optical frequency shift distribution with the sensing resolution of a 5 mm at 104 m fibre end (d) Corresponding distribution function (CDF) of the random frequency shifts

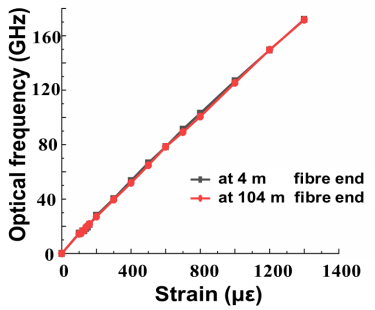

Fig.6 The relationship between the applied strain and the optical frequency shift

the accuracy is about 125.6 MHz with the 5 mm resolution and 499.7 MHz with the 2mm resolution.

Besides the nonlinear sweep noise and random sweep range, the intrinsic laser phase noise and system intensity noise will deteriorate with the increasing length of fibre under test. The spatial resolution with the long-distance fibre will be expanded by the nonlinear sweep noise and phase noise simultaneously. Moreover, the increasing beat frequency of the long-distance OFDR restrains the compensation of the nonlinear sweep noise. It is noted that the length of the fixed optical path delay in the auxiliary interferometer has to be twice the fibre under test. Therefore, no information can be detected beyond 95 m with 190 m optical fibre length by the conventional OFDR. Here, the frequency interval of $\pi/4$ in the Hilbert transform of the proposed method can realise a 100 m distributed sensing. Fig. 5(a) shows the spectrum distribution with 104 m fibre under test. The equal frequency resample enables a 46.3 μm spatial resolution at 102 m fibre by efficiently suppressing the nonlinear sweep noise (Fig.5 (b)). Corresponding distributed strain measurement is presented in Fig.5 (c). The sensing resolution is 5 mm. The increasing deviation of frequency shift proves the phase noise and inaccurate compensation of the nonlinear sweep noise. However, the obtained accuracy is still high to 458.2 MHz with the 5 mm resolution at the 104 m fibre end, as shown in Fig.5 (d).

The sensitivity coefficient between the applied strain and the induced optical frequency shift needs to be studied for the actual strain sensing accuracy. The average value of the optical frequency shift in the strained fibre section is used to avoid frequency deviation. The relationship between the applied strain and the corresponding optical frequency shift is shown in Fig. 6. A 5 mm sensing resolution is utilised for a more uniform measurement distribution. The slope of the curve represents the strain sensitivity coefficient, indicating the linearity between the applied strain and the corresponding frequency shift. The slope at the 4 m fibre end is 123.8 MHz/με, while the slope at 104 m is 123.1 MHz/με. The long-distance sensing barely affects the sensitivity coefficient. The R-square, the coefficient of determination, is introduced to represent the linearity of the strain sensitivity coefficient. The value of R-square is 0.9994 at the 4 m fibre end and 0.9989 at the 104 m fibre end in Fig.6, proving the high fidelity and linearity between the applied strain and measured frequency shift. Therefore, with a 5 mm resolution, the measurement strain accuracy is ±0.51 με at 4 m fibre length and ±1.86 με at the 104 m fibre length. The corresponding strain accuracy is ±2.01 με with 2 mm resolution

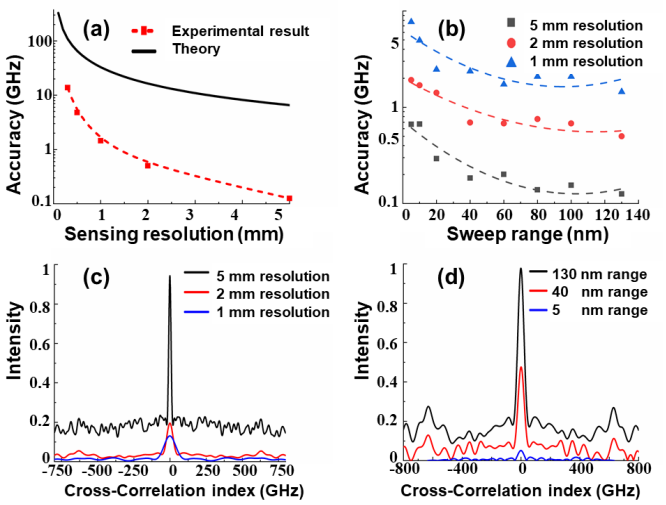

Fig.7 (a) Theoretical and experimental relationship between the accuracy and sensing resolution (b) Measurement accuracy with various wavelength sweep range (c) Distribution of cross correlation with different sensing resolution (d) Distribution of cross correlation with different sweep range

and 4 m fibre length.

A. Relationship between strain accuracy and resolution

Spatial frequency filtering in the OFDR, as slidewindow, is designed for obtaining characterisation of local Rayleigh spectrum at the specific position. The cross correlation between the reference and measurement is:

$$I_j^{(1)'} \otimes I_{N'-j}^{(2)*'} = \frac{1}{2\pi N'} \sum_{m=m_1}^{m_2} \tilde{I}_m^{(1)} \tilde{I}_m^{(2)*} \exp\left(ijm\frac{2\pi}{N'}\right) \quad (5)$$

where $\tilde{I}_m^{(1)}$ and $\tilde{I}_m^{(2)}$ are the reference and measurement frequency domain signal after spatial frequency filtering. It is noted that the strain-induced frequency shift is derived based on the whole sweep wavelength range. Therefore, there is a trade-off between the strain resolution and sensing length resolution [8]:

$$L_{res}\varepsilon_{res} = \lambda/(4n) \quad (6)$$

where ε_{res} is strain resolution, and L_{res} is the sensing resolution. Take a 130 nm sweep range and a 5 mm resolution for example. One single spatial frequency filtering contains 793 theoretical points. Therefore, the frequency resolution is 20.5GHz. On the other hand, with the desired accuracy of 1 με and the strain sensitivity coefficient of 123 MHz/με, the corresponding frequency accuracy should be 123 MHz. Therefore, the theoretical relationship in Eq.6 has set the limitation of the measurement accuracy and sensing resolution. Padding zeros to the filtered spatial domain signals can improve the optical frequency measurement resolution [18]. But it will also encounter some intrinsic noise, such as phase noise, nonlinear sweep noise and random position deviation noise. Thus, the experimental relationship between accuracy and sensing resolution based on the proposed method has been studied and shown in Fig. 7(a). The sweep wavelength range is 130 nm. The experimental accuracy of 125.6 MHz is beyond the theoretical limitation of 6.572 GHz with a sensing resolution of 5 mm. The realisation of such high accuracy proves the effectiveness of suppression of nonlinear sweep noise and random sweep range. The accuracy deteriorates exponentially with the decreasing resolution. It is reduced to 1.46GHz with a resolution of 1mm, corresponding to the ±5.89 με strain accuracy. The accuracy is further up to 13.815 GHz with a resolution of 0.3 mm.

Improving sweep range is one of the most straightforward ways to improve the measurement accuracy because it can reduce the theoretical step for the high signal to noise ratio in the cross-correlation. A 130 nm sweep range can provide 6.3 μm spatial resolution, while a 5 nm sweep range can only provide 164 μm spatial resolution. The relationship between sweep range and measurement accuracy is shown in Fig. 7(b). Measurement accuracy deteriorates with the smaller sweep range. When the sweep range is 5 nm, and the sensing resolution is 1 mm, there are only 6 points within one slide window. The measurement accuracy is still limited to 7.693 GHz, while the theoretical prediction of accuracy is 104.16

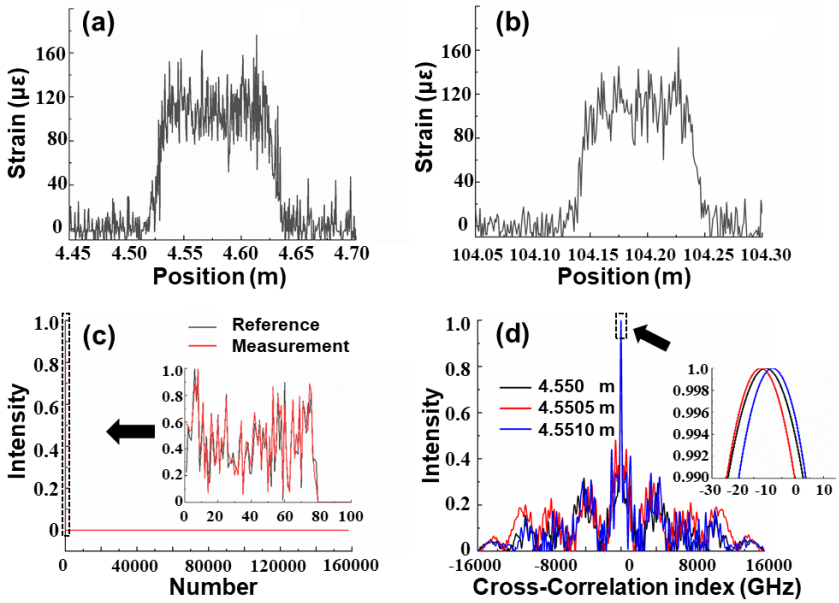

Fig.8 (a) Distribution of strain measurement with the sensing resolution of 0.5 mm at 4 m fibre (b) Distribution of strain measurement with the sensing resolution of 1 mm at 104 m fibre (c) Spectrum distribution after slidewindow and padding zeros (d) Random cross correlation peaks at the nearby fibre segment

GHz, about 14 times improvement beyond the theory. The performance of cross-correlation is a decisive factor for the high accuracy OFDR. Signal to noise ratio and bandwidth of the cross-correlation is studied with various sensing resolutions and sweep ranges. Normalise intensity distribution of the cross-correlation is shown in Fig. 7(c) with the fixed sweep range of 130 nm. The reduced sensing resolution deteriorates the signal to noise ratio and expands the bandwidth of cross-correlation peaks. Fig. 7(d) represents the influence of the sweep range at a sensing resolution of 2 mm. Signal to noise ratio is deteriorated by the decreasing sweep range, which barely affects the bandwidth of cross-correlation.

B. Further sub-millimetre sensing resolution

The strain distribution with the further reduced sensing resolution is discussed in Fig. 8. With a 0.5 mm sensing resolution and 100 με applied strain, the measurement frequency accuracy is 4.78 GHz. The corresponding strain accuracy is ±19.31 με (Fig. 8(a)). The strain distribution with a long-distance fibre of 104 m is also shown in Fig. 8(b). The strain accuracy is about ±8.72 με, while the sensing resolution is 1 mm and applied strain is 100 με. To our knowledge, this is the best strain accuracy realisation with such a fibre length and resolution.

The theoretical relationship between accuracy and sensing resolution has been discussed above. For the submillimetre resolution, the effective number of theoretical spatial steps is greatly restrained. In the 0.5 mm sensing resolution in Fig. 8(a), the corresponding sweep range is 130 nm. The individual frequency shift of one theoretical step is about 204.75GHz. There are only 79 effective points within one 0.5 mm slidewindow filtering, as shown in the inset of Fig. 8(c).

On the other hand, for the required measurement accuracy of 1 με, the corresponding accuracy of frequency shift needs to be 128.3MHz. Therefore, 1595 times of zeros need to be padded after one slidewindow spatial frequency filtering. In Fig. 8(c), the practical number of one slidewindow is almost 160,000. The cross-correlations of 3 successive fibre segments under the resolution of 0.5 mm are shown in Fig. 8(d), of which the positions are 4.5500m, 4.5505m and 4.5510m, respectively. The applied stain is 100 με. Measured frequency shifts are shown in the inset of Fig. 8(d). The corresponding measured peaks are 10.69 GHz, 12.59 GHz and 8.12 GHz. The random deviation can still be regarded as the limitation of effective number in one slidewindow. Before cross-correlation, the direct determinant factor is the accurate calculation of spatial frequency components within one slide window, as the 79 points shown in Fig. 8(c). Thus, besides the effective suppressed nonlinear sweep noise and the random wavelength range in this paper, the intrinsic noise, such as laser phase noise, intensity noise and bandwidth of digitiser, may need to be investigated for further accuracy improvement.

IV. CONCLUSION

Theoretical spatial resolution and the same physical fibre segment comparison for the cross-correlation are the most critical factors for the high accuracy with the extreme sensing resolution in OFDR. By effective suppressing the nonlinear wavelength sweep and random sweep range, we have delivered several με-level accuracy under millimetre/ submillimetre resolution. The 100-meter distributed strain sensing with a 1 mm resolution and ±8.72 με accuracy are also realised.

Such sensing accuracy with mm/sub-mm resolution is obtained at the expense of amounts of data processing. For the practical application, sweep range, length of fibre under test and sampling rate still need careful designation and optimisation to reduce the response time of the proposed OFDR interrogator. Realising high accuracy with ultimate sensing resolution can further enhance the distributed optical fibre sensing to some new potential applications, such as a medical image and battery manager monitoring. Besides, with a further demand of accuracy and/or resolution, such as one με accuracy under 0.1 mm sensing resolution, the intrinsic phase noise and intensity noise may become the predominant limitation.

REFERENCE

[1]. W. Eickhoff and R. Ulrich, "Optical frequency domain reflectometry in single-mode fiber," *Appl. Phys. Lett.*, vol. 39, no. 9, pp. 693–695, 1981.

[2]. R. Passy, N. Gisin, J. P. von der Weid, and H. H. Gilgen, "Experimental and theoretical investigations of coherent OFDR with semiconductor laser sources," *J. Lightwave Technol.*, vol. 12, no. 9, pp. 1622–1630, 1994.

[3]. A. Minardo, R. Bernini, R. Ruiz-Lombera, J. Mirapeix, J. Lopez-Higuera, and L. Zeni, "Proposal of Brillouin optical frequency-domain reflectometry (BOFDR)," *Opt. Express*, vol. 24, pp. 29994-30001, 2016.

[4]. U. Glombitza and E. Brinkmeyer, "Coherent frequency-domain reflectometry for characterization of single-mode integrated-optical waveguides," *Journal of Lightwave Technology*, vol. 11, no. 8, pp. 1377-1384, 1993.

[5]. J. Huang, L. A. Blanquer, J. Bonefacino, E. R. Logan, D. A. D. Corte, C. Delacourt, B. M. Gallant, S. T. Boles, J. R. Dahn, H.-Y. Tam, and J.-M. Tarascon, "Operando decoding of chemical and thermal events in commercial Na(Li)-ion cells via optical sensors," *Nature Energy*, vol. 5, no. 9, pp. 674–683, 2020.

[6]. Y. Yu, E. Vergori, D. Worwood, Y. Tripathy, Y. Guo, A. Somá, D. Greenwood, and J. Marco, "Distributed thermal monitoring of lithium ion batteries with optical fibre sensors," *Journal of Energy Storage*, vol. 39, p. 102560, 2021.

[7]. G. Han, J. Yan, Z. Guo, D. Greenwood, J. Marco, and Y. Yu, "A review on various optical fibre sensing methods for batteries," *Renew. Sustain. Energy Rev.*, vol. 150, no. 111514, p. 111514, 2021.

[8]. M. Froggatt and J. Moore, "High-spatial-resolution distributed strain measurement in optical fiber with rayleigh scatter," *Appl. Opt.*, vol. 37, no. 10, pp. 1735–1740, 1998.

[9]. C. Wang, K. Liu, Z. Ding, J. Jiang, Z. Chen, Y. Feng, Y. Zheng, Q. Liu, and T. Liu, "High Sensitivity Distributed Static Strain Sensing Based on Differential Relative Phase in Optical Frequency Domain Reflectometry," *Journal of Lightwave Technology*, vol. 38, no. 20, pp. 5825–5836, 2020.

[10]. H. Li, Q. Liu, D. Chen, and Z. He, "Centimeter spatial resolution distributed temperature sensor based on polarization-sensitive optical frequency domain reflectometry," *J. Lightwave Technol.*, vol. 39, no. 8, pp. 2594–2602, 2021.

[11]. S. Zhao, J. Cui, Z. Wu, Z. Wang, and J. Tan, "Distributed fiber deformation measurement by high-accuracy phase detection in OFDR scheme," *J. Lightwave Technol.*, vol. 39, no. 12, pp. 4101–4108, 2021.

[12]. K. Yuksel, M. Wuilpart, and P. Mégret, "Analysis and suppression of nonlinear frequency modulation in an optical frequency-domain reflectometer," *Opt. Express*, vol. 17, no. 7, pp. 5845–5851, 2009.

[13]. B. Soller, D. Gifford, M. Wolfe, and M. Froggatt, "High resolution optical frequency domain reflectometry for characterization of components and assemblies," *Opt. Express*, vol. 13, no. 2, pp. 666–674, 2005.

[14]. T.-J. Ahn, J. Y. Lee, and D. Y. Kim, "Suppression of nonlinear frequency sweep in an optical frequency-domain reflectometer by use of Hilbert transformation," *Appl. Opt.*, vol. 44, no. 35, pp. 7630–7634, 2005.

[15]. Z. Guo, G. Han, J. Yan, D. Greenwood, J. Marco, and Y. Yu, "Ultimate spatial resolution realisation in optical frequency domain reflectometry with equal frequency resampling," *Sensors*, vol. 21, no. 14, p. 4632, 2021.

[16]. M. Luo, J. Liu, C. Tang, X. Wang, T. Lan, and B. Kan, "0.5 mm spatial resolution distributed fiber temperature and strain sensor with position-deviation compensation based on OFDR," *Opt. Express*, vol. 27, no. 24, pp. 35823–35829, 2019.

[17]. K. Feng, J. Cui, D. Jiang, H. Dang, Y. Jin, X. Sun, Y. Niu, and J. Tan, "Improvement of the strain measurable range of an OFDR based on local similar characteristics of a Rayleigh scattering spectrum," *Optics Letters*, vol. 43, no. 14, p. 3293, 2018.

[18]. J. Cui, S. Zhao, D. Yang, and Z. Ding, "Investigation of the interpolation method to improve the distributed strain measurement accuracy in optical frequency domain reflectometry systems," *Appl. Opt.*, vol. 57, no. 6, pp. 1424–1431, 2018.

[19]. S. Zhao, J. Cui, Z. Wu, and J. Tan, "Accuracy improvement in OFDR-based distributed sensing system by image processing," *Opt. Lasers Eng.*, vol. 124, no. 105824, p. 105824, 2020.

[20]. P. Li, C. Fu, B. Du, J. He, H. Zhong, C. Du, L. Wang, and Y. Wang, "High-Spatial-Resolution Strain Sensor Based on Distance Compensation and Image Wavelet Denoising Method in OFDR," *Journal of Lightwave Technology*, vol. 39, no. 19, pp. 6334–6339, 2021.